applied sciences

MDPI

Article

Measurement of the Instrumental Effect Caused by Flexure Clamping on Quartz Crystal Microbalances

Diego Scaccabarozzi [1,*], Chiara Martina [1], Bortolino Saggin [2] and Emiliano Zampetti [3]

[1] Mechanical Engineering Department, Politecnico di Milano, 20156 Milano, Italy; chiara.martina@polimi.it
[2] Industrial Engineering Department, CISAS—Università degli Studi di Padova, 35131 Padova, Italy; bortolino.saggin@unipd.it
[3] Institute of Atmospheric Pollution Research—CNR, 00010 Rome, Italy; emiliano.zampetti@cnr.it
* Correspondence: diego.scaccabarozzi@polimi.it

Abstract

This study focuses on piezoelectric quartz crystal microbalances (QCMs), widely used in space and military instrumentation, as fundamental components in highly sensitive mass detection devices. In this research, a proper setup was developed to investigate the relationship between clamping preload and crystal resonance, with particular attention to the effects of concentrated loads. The latter ones, not properly addressed in the literature, come from the need to safely clamp QCMs in critical environments, like those experienced during the launch of rockets or payloads. Thus, the study investigates the behaviour of piezoelectric quartz crystals (AT-cut, 10 MHz) with gold electrodes, using a QCMs' three-pinned mounting system. Measurements showed that the effect of the preload on the frequency variation resulted in a repeatable increase in the crystals' resonance, increasing the loading, up to three ppm more than the unloaded quartz crystal oscillating frequency.

Keywords: QCM; mechanical preload; concentrated loads; mounting system; frequency stability

Academic Editor: Ephraim Suhir

Received: 13 June 2025
Revised: 14 July 2025
Accepted: 21 August 2025
Published: 22 August 2025

Citation: Scaccabarozzi, D.; Martina, C.; Saggin, B.; Zampetti, E. Measurement of the Instrumental Effect Caused by Flexure Clamping on Quartz Crystal Microbalances. *Appl. Sci.* **2025**, *15*, 9261. https://doi.org/10.3390/app15179261

1. Introduction

Quartz oscillators are fundamental components in many different military and space applications due to their high precision and reliability; for instance, they are mainly integrated into mission payloads that require highly accurate timing, such as in communication and navigation systems, ultra-precise clocks [1,2], and to develop mass sensors as Quartz Crystal Microbalances (QCMs), are often utilized as thickness-shear mode resonators combined to thermogravimetric analyses [3–6].

QCMs are typically used in space/aerospace applications, such as in satellites to monitor the deposition of dust, material outgassing, and degradation of spacecraft materials or in the field of earth observation to monitor pollutants in the atmosphere [7–10]. QCMs have proven essential in space missions by providing real-time measurements of the mass of contaminants, ensuring that sensitive equipment such as optical lenses, sensors, and solar panels remain unaffected by space debris and contamination [11–21].

The working principle of QCM instruments is based on the piezoelectric properties of quartz; when an oscillating electric field is applied to a quartz disk by integrated electrodes, it deforms, creating mechanical oscillations as thickness-shear modes, for AT-cut quartz [22–24].

Piezoelectric crystals in microbalances allow the measurement of the mass of the materials deposited on electrodes by computing the variation in the crystal's resonant frequency using the Sauerbrey equation (Equation (1)) as a transduction model [25]:

$$\Delta f_m = -\Delta m \frac{2{f_0}^2}{A\sqrt{G\rho_c}} \quad (1)$$

In the Sauerbrey equation, Δfm represents the change in resonant frequency measured after the mass deposition, Δm denotes the deposited mass, f_0 is the fundamental frequency of the quartz crystal disk, and A, G and ρc correspond to the active area, the shear modulus, and the density of the quartz, respectively.

The stability of the oscillating frequency is mandatory for instrument performance in many high-precision applications, such as biosensing and soft-matter research, food and quality assurance, gas sensing, and space contaminants monitoring. Several factors can influence frequency stability, including temperature, humidity, pressure, acceleration and vibration, magnetic field, electric field, external distributed load, and radiation [8,26–31].

In the context of space applications, where environmental conditions can sharply change, understanding the factors that contribute to frequency instability is essential; for instance, temperature effects can alter the physical properties and the piezoelectric behaviour of the quartz crystal, which in turn affects the frequency response [32–35]. The latter is generally accommodated by proper instrument calibration, measuring the frequency variation within the temperature range of interest.

Moreover, payload instruments on space missions must operate reliably across wide temperature ranges, resulting in varying thermoelastic stress conditions [36–39]. In the specific case of microbalances, thermal variations can alter the mechanical preload on the crystals due to different thermal expansions of the mounting system materials, since they can operate at environmentally cryogenic temperatures as well as in higher temperature conditions, i.e., up to 60 °C [40–42]. It is therefore essential to study how these temperature variations affect device performance, whether they induce frequency shifts that could affect the signal, and to quantify these effects.

Despite increasing usage of QCMs in space applications, the effect of concentrated loads on quartz crystals has not been addressed yet in the literature; concentrated loads are mandatory to hold the QCMs in critical environments, like the ones related to space applications, due to high vibration levels and/or large temperature variations [43–45].

Furthermore, the mechanical preload applied by the oscillator mounting system, particularly when the quartz oscillating area is close to the holder, can introduce localised stress on the crystal. This stress may lead to fluctuations in the oscillator frequency, a phenomenon acknowledged in the literature but rarely characterised experimentally, with most studies focusing primarily on radial force applications [46–49]. Moreover, for the biosensing application of QCMs, the observed influence of mechanical loading on frequency response suggests that similar effects could occur in sensitive measurements, potentially mimicking or obscuring subtle interfacial phenomena. These insights can inform calibration protocols and sensor mounting strategies aimed at minimising mechanical artefacts, thereby improving measurement fidelity in various QCM-D applications [50,51].

Thus, the research experimentally evaluates the effect of concentrated loads on the oscillating frequency of QCMs to quantify the measurement error in such conditions.

The latter information is relevant to assessing the uncertainty budget contribution in QCM measurements. Section 2 describes the measurement methodology, focusing on the developed measurement setup, and Section 3 summarises the experimental results. Section 4 discusses the main findings of the research, and Section 5 concludes the paper.

2. Materials and Methods

The study focuses on the mounting system of a QCM already studied for being a spacecraft payload [12], where the quartz crystal is underpinned in three contact points spaced 120° apart.

The QCM under investigation is a 10 MHz AT-cut quartz crystal disk equipped with two circular gold electrodes, one on the top and one on the bottom surface, providing the necessary input to induce thickness-shear mode vibrations. The main geometrical dimensions of the crystal are reported in Table 1, such as the diameter and the thickness of the quartz disc and the diameter of the two electrodes.

Table 1. Geometric dimensions.

Parameter	Value
Electrodes diameter	6.0 ± 0.2 mm
Quartz disc diameter	13.95 ± 0.001 mm
Thickness of the disc	0.167 ± 0.001 mm
Preloading element stiffness	7.9 ± 1.3 N/mm
Clamping preload	1.7 N

A preliminary experimental characterisation of the stiffness of the flexure holding structure at room temperature was performed. Ten trials were conducted on different samples, each involving a series of ten controlled displacement inputs (with 0.01 mm steps provided by a micrometric screw). During each trial, the resulting force was measured using a load cell. For each test, a linear regression was performed as illustrated in Figure 1, the linear relationship between the applied displacement (x-axis) and the measured force (y-axis) was confirmed along with all the tests performed.

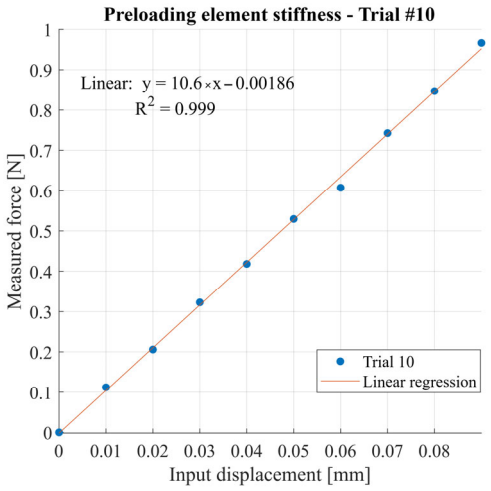

Figure 1. Experimental characterisation of the preloading element stiffness, Trial #10.

The measured mechanical stiffnesses are summarised in Table 2, reported as the mean value along with the associated measurement uncertainty. The experimental results are in good agreement with the numerical predictions by FEM analyses [14], with a maximum deviation of less than 9.2%, which is considered acceptable within the mechanical geometrical tolerances.

Table 2. Summary of the experimental characterisation of the preloading element mechanical stiffness.

Trial Number	Value [N/mm]	R^2
#1	9.37	0.994
#2	8.78	0.997
#3	6.77	0.983
#4	6.34	0.977
#5	6.64	0.970
#6	7.76	0.992
#7	7.51	0.994
#8	7.45	0.999
#9	8.16	0.997
#10	10.60	0.999
Average value	7.9	-
Measurement uncertainty	1.3	-
Theoretical value	7.26	-

A scheme of the testing setup is shown in Figure 2, and Figure 3 highlights the view of the supporting structure and assembled crystal under testing [52] beside the additional elements of the developed setup.

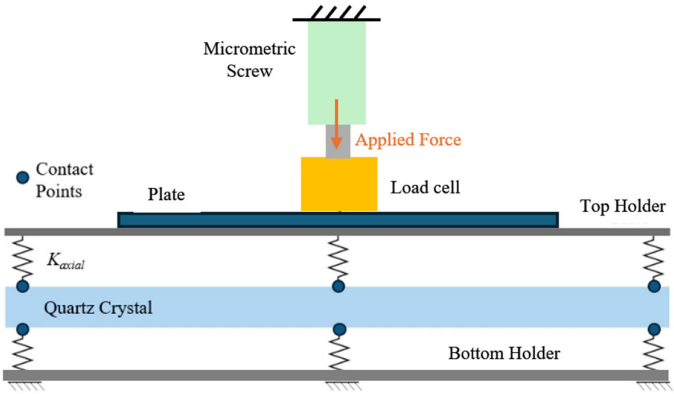

Figure 2. Scheme of the testing setup with details of the mechanical holding and preloading system, load cell and micrometric screw.

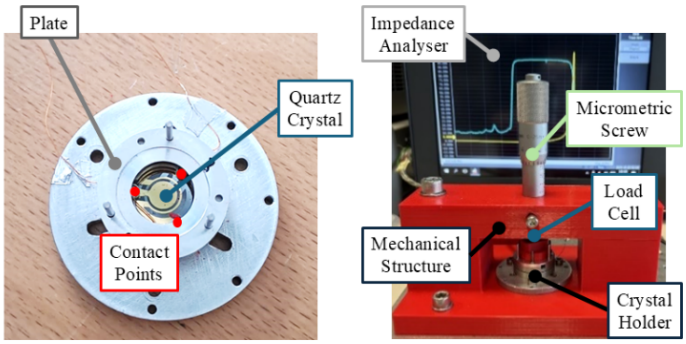

Figure 3. (**Left**) view of the tested item with the mechanical supporting structure and the contact points; (**right**) view of the testing setup with the main elements for the preload effect measurement.

The force is transmitted through a micrometric screw (Mitutoyo 150–190 model) to the load cell (Honeywell FS Series Force Sensor PK 88870, Honeywell, Charlotte, NC, USA, with 15 N full scale), which is directly connected on an aluminium plate, distributing the force uniformly on the QCM top holder. The latter element transmits the force to the

quartz crystal through compliant elements whose stiffness evaluation (K_{axial}) is given in Tables 1 and 2.

The overall force is distributed on three points of the quartz crystal, which is kept below by a holder with similar geometry and compliant elements (i.e., the bottom holder). The setup comprises three mechanical guides that ensure the perpendicular application of the load controlled by the micrometric screw, preventing the crystal from slipping.

The crystal is connected to an electronic oscillator circuit used to sustain the oscillation and obtain the QCM output signal, i.e., a TTL signal having a frequency equal to the fundamental crystal resonating frequency. This configuration reproduces the typical measurement system of a conventional microbalance QCM [53–57].

The measurement chain is schematized in Figure 4 through a block scheme; an HP Agilent Keysight E3647A (Agilent, Santa Clara, CA, USA) power supply provided the necessary current and voltage to the oscillator circuit. An HBM Scout 55 amplifier was connected to the force transducer and enabled the reading of the output voltage signal of the load cell. A National Instruments (National Instruments, Austin, TX, USA) acquisition board (NI 9234 4 AI, ±5 V, 24-bit, 51.2 kS/s/ch Simultaneous, AC/DC Coupling, IEPE AC Coupling) was used to collect measured force, which was then processed on a PC.

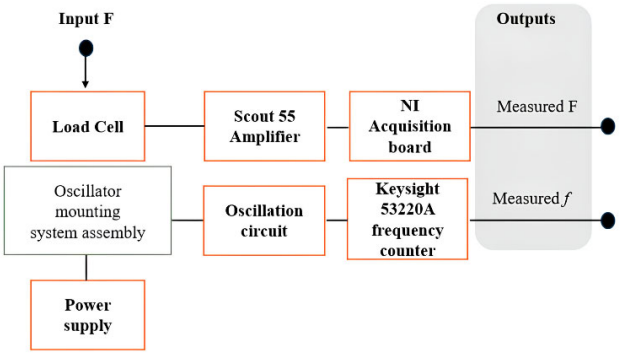

Figure 4. Scheme of the measurement chain.

Furthermore, a Keysight 53220a (Keysight, Santa Rosa, CA, USA) universal frequency counter was added to the setup to measure the oscillator frequency signal, with a sampling rate of 1 Hz. The selected rate was sufficient for analysing static conditions, such as frequency shifts caused by the application of static and concentrated loads.

Moreover, a Keysight E4990A Impedance Analyzer was used to measure the quartz crystal admittance, both in unloaded and preloaded conditions, for comparison and verification of the test results from the frequency counter [58–60].

2.1. Load Cell Calibration

The force transducer was verified using static procedures by applying controlled loads (dead masses from 50 g to 500 g) to cover a force range of about 5 N. The load calibration was deemed necessary to evaluate the accuracy of the sensor in the reduced measurement force range. The calibration procedure was based on three loading and unloading cycles. The Scout 55 was configured with the following parameters: the load cell was operated in a full bridge configuration with an excitation voltage of 1.0 V. The input range was set to 1000 mV/V, and a digital low-pass filter with a cutoff frequency of 4 Hz was applied to reduce signal noise. Amplifier calibration was performed automatically, resulting in a nominal output range of 10 V and a corresponding calibration factor of 54.177 V/V. Measured data were analysed using linear regression. Results for each cycle, and considerations of the overall data, are summarised in Table 3.

Table 3. Load cell calibration result.

Test Number	Sensitivity (V/N)	Uncertainty (V/N)	R^2
1	0.2521	2.8×10^{-3}	0.9992
2	0.2470	4.4×10^{-3}	0.9980
3	0.2556	2.3×10^{-3}	0.9995
all dataset	0.2516	1.8×10^{-3}	0.9987

The sensitivity was found to have a small relative uncertainty, limited to a worst case of 1.8% of the measured value. The transducer's linearity was confirmed as well, as the linear regression provided a minimum R^2 value of 0.9980.

Considering the entire dataset, the best performance is achieved when the measured sensitivity was found to be (0.2516 ± 0.0018) V/N. Moreover, the analysis of the repeated calibration demonstrated a generally good repeatability of the sensor, with a standard deviation of the measured sensitivity set to 1.7% of the average value. The obtained result demonstrated the usability of the sensor to accurately measure the force during testing.

2.2. Testing Procedure and Data Analyses

The testing procedure consisted of performing controlled loading and unloading cycles on the QCM support and acquiring the frequency by using the frequency counter. Two quartz crystals (hereafter named "Crystal A" and "Crystal B") were tested in ambient pressure conditions and at a constant temperature (25 ± 1 °C).

However, it should be noted that the effect of the temperature fluctuation in the room is negligible in terms of frequency stability for the used AT-cut crystal. Each crystal was loaded and unloaded via the micrometric screw in steps of 0.4 N $\pm$ 0.1 N, performing five cycles in total. The test was named from 1A to 5A, and from 1B to 5B, for crystal A and crystal B, respectively. The last two test cycles on crystal A (i.e., the numbers 4A and 5A) were performed after a complete unloading step and switching off the instrumentation; the crystal was not dismounted, and tests were performed after a few days, aiming to evaluate measurement repeatability at different times.

It must be noticed that tests 4B and 5B were executed after having dismounted and remounted the crystal on the system. This adjustment aimed to evaluate the reproducibility of the frequency response across different mounting conditions and investigate the potential impact of repositioning on the measured resonant frequency shifts. The sampling frequency for the force was set to 1 Hz, as it was for the frequency counter. No filtering was applied during data processing, and for all the tested conditions, 15 data points were used to calculate the mean and standard deviation of the frequency and force values.

Then, the relative frequency variation $\Delta f/f_0$, defined as the normalised difference between the measured frequency in different loading conditions and the nominal oscillating frequency f_0 (set to 10 MHz) was evaluated:

$$\frac{\Delta f}{f_0} = \frac{f - f_0}{f_0} \tag{2}$$

Eventually, the correlation between the computed $\Delta f/f_0$ values was assessed through linear regression analysis.

3. Experimental Activity

An example of the signals acquired over time is shown in Figure 5, which illustrates the signals acquired by the load cell and the frequency counter during a loading cycle. Figures 6 and 7 highlight the frequency trend versus the measured applied force for the

acquired datasets of crystal A and B, whereas Table 4 summarises the measured frequency variations and the force statistics for the tested items.

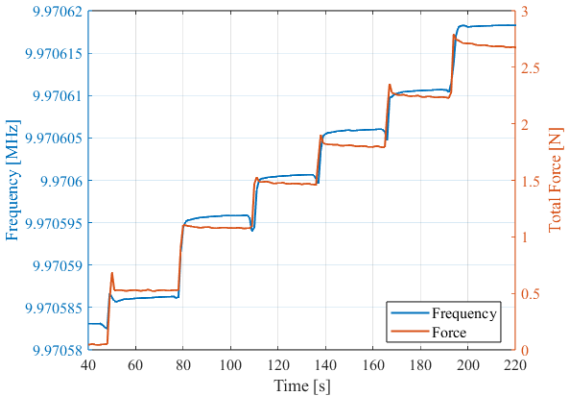

Figure 5. Example of acquired signals during a loading cycle.

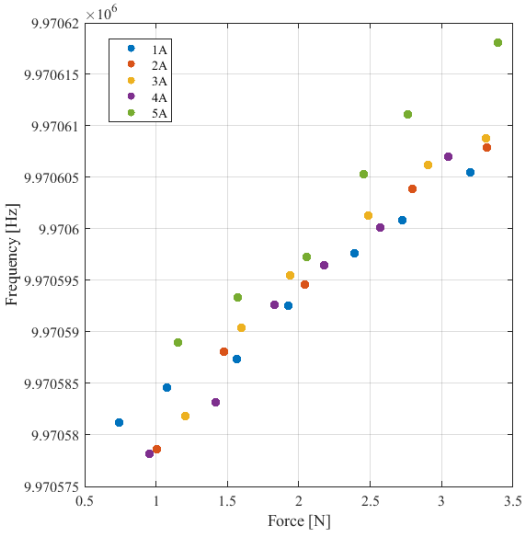

Figure 6. Measured frequency vs. force, data set for crystal A.

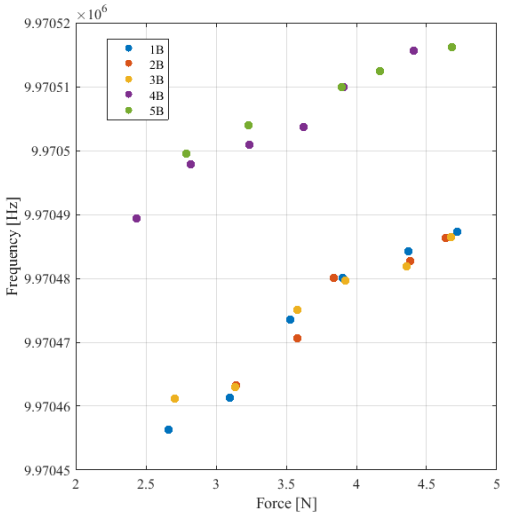

Figure 7. Measured frequency vs. force, data set for crystal B.

Table 4. Measured frequency vs. applied force, crystal A and B.

Test	Nominal Values	1	2	3	4	5	6	7	Worst Case Uncertainty (1σ%)
1A	Force [N]	0.76	1.08	1.57	1.93	2.40	2.72	3.20	0.27%
	Frequency [MHz]	9.970581	9.970585	9.970587	9.970593	9.970598	9.970601	9.970605	0.0000010%
2A	Force [N]	1.01	1.48	2.04	2.79	3.32	n.a.	n.a.	0.31%
	Frequency [MHz]	9.970578	9.970588	9.970594	9.970603	9.970607	n.a.	n.a.	0.0000012%
3A	Force [N]	1.20	1.60	1.94	2.48	2.91	3.31	n.a.	0.25%
	Frequency [MHz]	9.970582	9.970590	9.970596	9.970601	9.970606	9.970609	n.a.	0.0000010%
4A	Force [N]	0.95	1.42	1.83	2.17	2.57	3.05	n.a.	0.30%
	Frequency [MHz]	9.970578	9.970583	9.970593	9.970596	9.970600	9.970607	n.a.	0.0000013%
5A	Force [N]	1.15	1.57	2.05	2.45	2.76	3.39	n.a.	2.40%
	Frequency [MHz]	9.970589	9.970593	9.970597	9.970605	9.970611	9.970618	n.a.	0.0000017%
1B	Force [N]	2.50	3.10	3.53	3.90	4.37	4.72	n.a.	0.24%
	Frequency [MHz]	9.970456	9.970461	9.970474	9.970480	9.970484	9.970487	n.a.	0.0000004%
2B	Force [N]	2.76	3.14	3.58	3.84	4.38	4.64	n.a.	0.26%
	Frequency [MHz]	9.970460	9.970463	9.970471	9.970480	9.970482	9.970486	n.a.	0.0000018%
3B	Force [N]	2.71	3.13	3.58	3.92	4.35	4.68	n.a.	0.30%
	Frequency [MHz]	9.970461	9.970463	9.970475	9.970480	9.970482	9.970487	n.a.	0.0000033%
4B	Force [N]	2.43	2.82	3.24	3.62	3.91	4.41	n.a.	0.28%
	Frequency [MHz]	9.970489	9.970498	9.970501	9.970504	9.970510	9.970516	n.a.	0.0000023%
5B	Force [N]	2.79	3.23	3.90	4.17	4.68	n.a.	n.a.	1.12%
	Frequency [MHz]	9.970500	9.970504	9.970510	9.970512	9.970516	n.a.	n.a.	0.000015%

Figure 8 shows the admittance modulus and phase measured for crystal A, considering test 1A, in two different preload conditions, and Figure 9 provides a detailed view of the admittance spectrum where the maximum is measured.

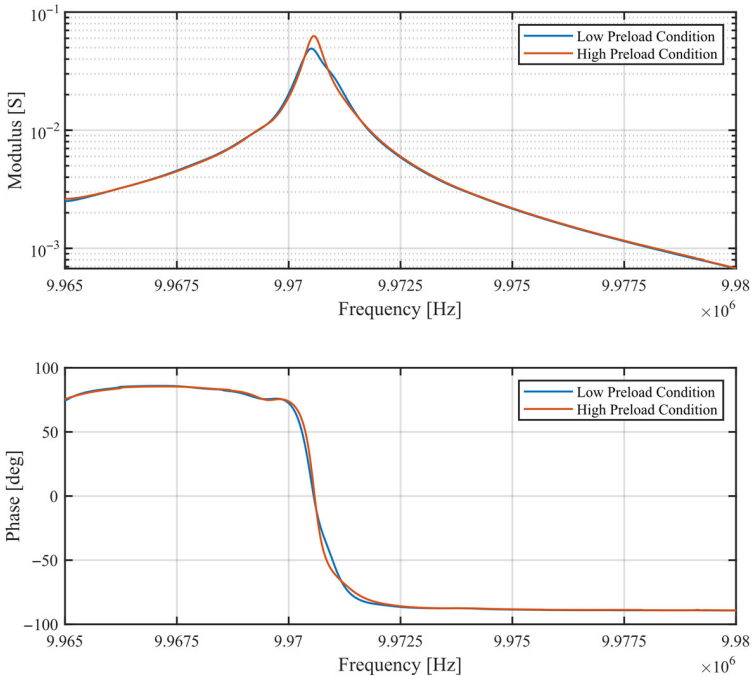

Figure 8. Modulus and phase diagrams of the crystal's admittance, measured in low (blue colour) and high (orange colour) preload conditions.

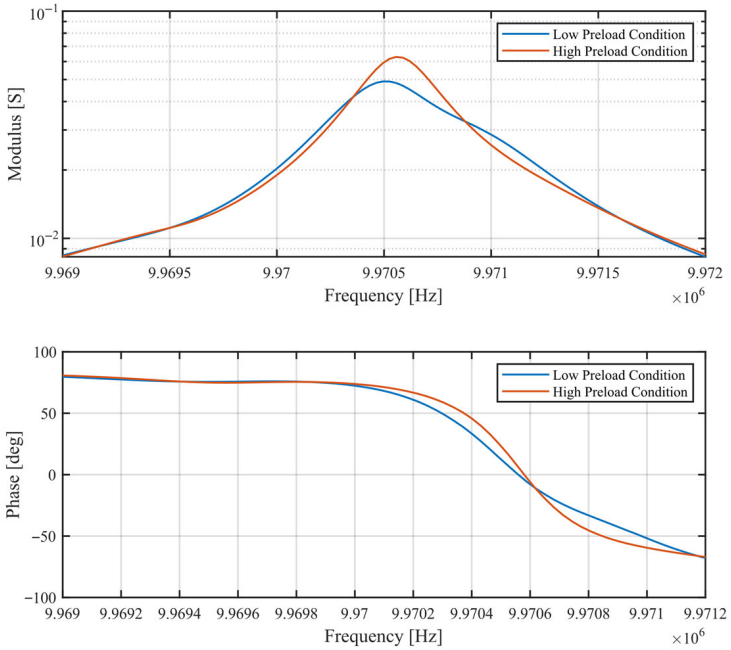

Figure 9. Detailed view of the modulus and phase diagrams of the crystal's admittance, measured in low (blue colour) and high (orange colour) preload conditions.

4. Discussion

As a general result, increasing the preload provided a repeatable and reproducible increase in the crystal's resonant frequency. This is highlighted by the collected dataset summarised in Table 4 and shown in Figures 6 and 7. Moreover, as illustrated in the graphs, data clustering occurred due to variations in the initial conditions of each test, which depend on the specific crystal being tested (A or B) and its positioning on the mounting system.

Analysing the dataset for crystal A, a good linear correlation of the $\Delta f/f_0$ with the preload was observed, as summarised in Table 5; the first three tests, i.e., from 1A to 3A, highlighted an average slope of 1.2420 10^{-6} N^{-1}, with a low relative standard deviation, set to 1% of the average value. Evaluating the repeatability of the measurement results, considering the entire dataset for crystal A, an increase in the measurement uncertainty of the relative frequency variation was observed, i.e., up to about 5.7% of the average value. The measured slope of the $\Delta f/f_0$ versus the applied force resulted in (1.296 $\pm$ 0.075) 10^{-6} N^{-1}.

Table 5. Linear regression of the dataset for crystal A.

Test	Slope [10^{-6} N^{-1}]	R^2
1A	1.2330	0.9740
2A	1.2451	0.9804
3A	1.2480	0.9688
4A	1.3960	0.9844
5A	1.3563	0.9818
Mean value	1.296	-
1σ	0.075	-
1σ (%)	5.7%	-

Analysing dataset B, worse linearity and repeatability were found. This is demonstrated either by computed R^2 or statistics, as shown in Table 6. Considering short-term repeatability, i.e., the tests from 1B to 3B, the measured slope of the $\Delta f/f_0$ was (1.48 $\pm$ 0.12) 10^{-6} N^{-1}, therefore providing a relative uncertainty of about 7.9% of the average value. Moreover, assessing the reproducibility of the testing procedure, i.e., considering the tests 4B and 5B after the dismounting and remounting of crystal B, an offset of the initial

frequency was measured (about 30 Hz) and an additional increase in the measurement uncertainty was obtained. Despite the dismounting of crystal B, the trend of the dataset retains consistency, confirming a direct effect between the concentrated applied load on the quartz crystal and its frequency shift.

Table 6. Linear regression of the dataset for crystal B.

Test	Slope [10^{-6} N^{-1}]	R^2
1B	1.5920	0.9585
2B	1.5022	0.9245
3B	1.3586	0.9500
4B	1.2523	0.9719
5B	1.4613	0.9489
Mean value	1.43	-
1σ	0.13	-
1σ (%)	9.2	-

Indeed, considering the overall measured data for crystal B, the obtained slope of the $\Delta f/f_0$ versus the applied force was (1.43 ± 0.13) 10^{-6} N^{-1}.

Comparing the results from the two datasets, it can be noticed that the measured slopes of $\Delta f/f_0$ are compatible, but in general with a difference of around 10% on the average values. The discrepancy can be attributed to defects in the quartz crystalline structure, while manufacturing tolerances and electrode deposition technology primarily account for the differences in the nominal resonance frequencies of the two crystals. These results confirm that, despite uncertainties related to the crystal structure and/or the fabrication process, the observed frequency shift consistently appears across all tested samples. In the future, microstructural analyses could be performed to investigate the measured discrepancy better.

The measured slope difference stresses the need to singularly evaluate the highlighted instrumental effect for each crystal, to enhance the accuracy of measurements with QCMs. Indeed, the increase in frequency occurred in all the tests performed, in the same order of magnitude, i.e., about 33 Hz at the highest loading condition. This variation can be relevant in the case of very high-precision applications, being about 30 times the typical frequency resolution of such devices. Considering general space applications, a typical operative condition which can cause the appearance of the highlighted instrumental effect is when the instrument is exposed to severe temperature ranges, for instance, down to cryogenic temperatures, commonly achieved on instruments and payloads facing cold scenarios without any active thermal control. In that condition (e.g., at −150 °C), the mounting system characterised in this work would cause a force variation of only about 0.5 N, therefore, well limiting the consequences of the measured instrumental effect. This is possible due to a proper design trade-off between axial rigidity, necessary to guarantee the mechanical robustness needed in the launch vibration environment, and the thermal compliance to cope with the temperature variation. However, different and stiffer designs might lead to higher preload force variation, even for lower temperature ranges. This confirms the relevance of the obtained results, stressing the need to account for and assess the measured instrumental effect starting from the preliminary design phases.

Moreover, a comparison with the applicable literature [49], where pin loads are applied in-plane to an AT-cut square quartz crystal of about 3.8 MHz, showed a general agreement with the obtained results, therefore supporting the robustness of the obtained findings.

Eventually, as previously mentioned, the admittance of the crystals was measured as well. As can be seen in Figure 8, the shape of the crystal admittance does not change significantly under different loading conditions. Indeed, the major effect observed is a rightward shift of the admittance maximum at the highest load, indicating an increase in the crystal's

resonance, in agreement with the data obtained from the frequency counter. However, the obtained results, focusing on the admittance modulus change, open the possibility to study how the spectral changes under preload, caused by the studied instrumental effect, could affect the measurements in other applications, like in QCM-D analyses of viscoelastic films, where the electrical impedance is generally monitored in tandem with the frequency.

5. Conclusions

The characterisation of the instrumental effect caused by concentrated loads from the clamping systems of crystal resonators was assessed in this study. A setup was designed to evaluate frequency shifts caused by a controlled, measured, concentrated load on the crystal, applied to AT-cut, 10 MHz quartz crystals with gold electrodes, and mounted in a three-point clamping system.

The study showed that the three-point clamping system, mandatory to hold the crystals in critical environments like the one experienced in space-related applications, causes an increase in the main resonance of about three ppm at the maximum applied loads (about 5 N with AT-cut 10 MHz crystal). Despite the measured effect not being critical for many applications, it can be relevant in the case of high-precision applications, as the measured maximum variation is about one order of magnitude of the usual frequency resolution of such devices.

Indeed, future activities will evaluate the investigated phenomenon, testing a larger number of samples to confirm the obtained results. Moreover, characterisation in low-pressure conditions will foster the development of quartz crystals and improved mechanical holding systems for high-precision space applications.

Author Contributions: Conceptualization, D.S. and C.M.; methodology, D.S., C.M., B.S. and E.Z.; validation, D.S., C.M., B.S. and E.Z.; formal analysis, C.M.; investigation, C.M. and D.S.; data curation, C.M. and D.S.; writing—original draft preparation, C.M.; writing—review and editing, D.S., E.Z. and B.S.; supervision, D.S. All authors have read and agreed to the published version of the manuscript.

Funding: The author declares that no funding was received for this work.

Institutional Review Board Statement: Not applicable.

Informed Consent Statement: Not applicable.

Data Availability Statement: The original contributions presented in this study are included in the article. Further inquiries can be directed to the corresponding author.

Acknowledgments: The authors would like to acknowledge Chiara Gisellu and Andrea Appiani for their contribution and support to the research activity.

Conflicts of Interest: The authors declare no conflicts of interest.

References

1. Norton, J.R.; Cloeren, J.M. Precision quartz oscillators and their use aboard satellites. *Johns Hopkins APL Tech. Dig.* **1994**, *15*, 30–37.
2. Lam, C.S. A review of the recent development of MEMS and crystal oscillators and their impacts on the frequency control products industry. In Proceedings of the 2008 IEEE Ultrasonics Symposium, Beijing, China, 2–5 November 2008; pp. 694–704. [CrossRef]
3. Mansfield, E.; Kar, A.; Quinn, T.P.; Hooker, S.A. Quartz crystal microbalances for microscale thermogravimetric analysis. *Anal. Chem.* **2010**, *82*, 9977–9982. [CrossRef] [PubMed]
4. Sai, N.; Tagawa, Y.; Sohgawa, M.; Abe, T. Miniature quartz crystal-resonator-based thermogravimetric detector. *Rev. Sci. Instrum.* **2014**, *85*, 095001. [CrossRef] [PubMed]
5. Vaughan, S.R.; Speller, N.C.; Chhotaray, P.; McCarter, K.S.; Siraj, N.; Pérez, R.L.; Li, Y.; Warner, I.M. Class-specific discrimination of volatile organic compounds using a quartz crystal microbalance-based multisensor array. *Talanta* **2018**, *188*, 423–428. [CrossRef]
6. Smith, A.L.; Mulligan, R.B., Sr.; Shirazi, H.M. Determining the effects of vapor sorption in polymers with the quartz crystal microbalance/heat conduction calorimeter. *J. Polym. Sci. B Polym. Phys.* **2004**, *42*, 3893–3906. [CrossRef]

7. Zampetti, E.; Macagnano, A.; Papa, P.; Bearzotti, A.; Petracchini, F.; Paciucci, L.; Pirrone, N. Exploitation of an integrated microheater on QCM sensor in particulate matter measurements. *Sens. Actuators A Phys.* **2017**, *264*, 205–211. [CrossRef]
8. Tsuchiya, Y.; Kukita, H.; Shiobara, T.; Yukumatsu, K.; Miyazaki, E. Temperature controllable QCM sensor with accurate temperature measurement for outgas and contamination assessment. In Proceedings of the 2019 IEEE SENSORS, Montreal, QC, Canada, 27–30 October 2019; pp. 1–4. [CrossRef]
9. Pérez, R.L.; Ayala, C.E.; Park, J.-Y.; Choi, J.-W.; Warner, I.M. Coating-Based Quartz Crystal Microbalance Detection Methods of Environmentally Relevant Volatile Organic Compounds. *Chemosensors* **2021**, *9*, 153. [CrossRef]
10. Yaroshenko, I.; Kirsanov, D.; Marjanovic, M.; Lieberzeit, P.A.; Korostynska, O.; Mason, A.; Frau, I.; Legin, A. Real-Time Water Quality Monitoring with Chemical Sensors. *Sensors* **2020**, *20*, 3432. [CrossRef]
11. Dirri, F.; Palomba, E.; Longobardo, A.; Zampetti, E.; Saggin, B.; Scaccabarozzi, D. A review of quartz crystal microbalances for space applications. *Sens. Actuators A Phys.* **2019**, *287*, 48–75. [CrossRef]
12. Scaccabarozzi, D.; Martina, C.; Saggin, B.; Junior, E.V.V.; Palomba, E.; Longobardo, A.; Gisellu, C.; Dirri, F.; Zampetti, E.; Pedone, M.; et al. Feasibility Design of DIANA, a Dust Analyzer developed for the Tianwen-2 Mission. In Proceedings of the 2024 11th International Workshop on Metrology for AeroSpace (MetroAeroSpace), Lublin, Poland, 3–5 June 2024; pp. 422–426. [CrossRef]
13. Martina, C.; Scaccabarozzi, D.; Saggin, B.; Vaz Junior, E.V.; Palomba, E.; Longobardo, A.; Gisellu, C.; Dirri, F.; Zampetti, E.; Pedone, M.; et al. DIANA, a cometary dust in-situ analyzer for Tianwen-2 mission: Thermomechanical design. In Proceedings of the 75th International Astronautical Congress (IAC), Milan, Italy, 14–18 October 2024. Paper IAC-24-A3.4B.
14. Martina, C.; Saggin, B.; Palomba, E.; Zampetti, E.; Mancuso, M.A.; Scaccabarozzi, D. Finite element modelling of thermoelastic behavior for high-temperature quartz crystal microbalance. In Proceedings of the 2023 IEEE 10th International Workshop on Metrology for AeroSpace (MetroAeroSpace), Milan, Italy, 19–21 June 2023; pp. 109–113. [CrossRef]
15. Shapira, A.; Stern, A.; Prazot, S.; Mann, R.; Barash, Y.; Detoma, E.; Levy, B. An Ultra Stable Oscillator for the 3GM experiment of the JUICE mission. In Proceedings of the 2016 European Frequency and Time Forum (EFTF), York, UK, 4–7 April 2016; pp. 1–5. [CrossRef]
16. Suliga, A.; Ergincan, O.; Rampini, R. Modeling of spacecraft outgassed contamination levels by thermogravimetric analysis. *J. Spacecr. Rocket.* **2021**, *58*, 1010–1016. [CrossRef]
17. Dushin, V.K.; Krylov, A.N.; Soares, C.E. On-orbit quartz crystal microbalance measurements of molecular deposition on Russian and US Space Stations. In Proceedings of the 25th International Symposium on Rarefied Gas Dynamics (RGD), St. Petersburg, Russia, 21–28 July 2006.
18. Wood, B.E.; Hall, D.F.; Lesho, J.C.; Dyer, J.S.; Uy, O.M.; Bertrand, W.T. Quartz crystal microbalance (QCM) flight measurements of contamination on the MSX satellite. In Proceedings of the SPIE's 1996 International Symposium on Optical Science, Engineering, and Instrumentation, Denver, CO, USA, 11 November 1996; Volume 2864.
19. Wood, B.; Bertrand, W.; Uy, M.; Lesho, J.; Cain, R.; Hall, D.; Green, B.; Galica, G.; Boies, M.; Dyer, J. Review of Midcourse Space Experiment (MSX) Satellite QCM Contamination Results After 8 Years in Space. In Proceedings of the 43rd AIAA Aerospace Sciences Meeting and Exhibit, Reno, NV, USA, 10–13 January 2005. [CrossRef]
20. Dawson, T.T.; Hill, C.A.; Rowell, A.F.; Leavor, K.R.; Hawley, S.A. SAGE III/ISS Contamination Monitoring Package: Observations in Orbit. NASA Technical Report, No. L-21120. 2020. Available online: https://ntrs.nasa.gov/api/citations/20205001963/downloads/NASA-TM-20205001963update.pdf (accessed on 20 August 2025).
21. Pereira, A.; Roussel, J.-F.; van Eesbeek, M.; Schmeitzky, O.; Faye, D. Experiments and Physical Modeling of Ultraviolet-Enhanced Contamination from Pure Contaminants. *J. Spacecr. Rocket.* **2006**, *43*, 402–409. [CrossRef]
22. Skládal, P. Piezoelectric Biosensors: Shedding Light on Principles and Applications. *Microchim. Acta* **2024**, *191*, 184. [CrossRef] [PubMed]
23. *ANSI/IEEE Std 176-1987*; IEEE Standard on Piezoelectricity. IEEE: New York, NY, USA, 1988. [CrossRef]
24. Shen, D.; Kang, Q.; Wang, Y.-E.; Hu, Q.; Du, J. New cut angle quartz crystal microbalance with low frequency–temperature coefficients in an aqueous phase. *Talanta* **2008**, *76*, 803–808. [CrossRef]
25. Sauerbrey, G. Use of quartz vibration for weighing thin films on a microbalance. *J. Phys.* **1959**, *155*, 206–212.
26. Cibiel, G.; Boizot, B.; Boy, J.J.; Carlotti, J.F.; Cambon, O.; Devautour-Vinot, S.; Piccheda, D. Ultra stable oscillators dedicated for space applications: Oscillator and quartz material behaviors vs radiation. In Proceedings of the 2006 IEEE International Frequency Control Symposium and Exposition, Newport Beach, CA, USA, 4–7 June 2006; pp. 814–822.
27. Yu, G.Y.; Janata, J. Proximity effect in quartz crystal microbalance. *Anal. Chem.* **2008**, *80*, 2751–2755. [CrossRef] [PubMed]
28. Park, K.; Koh, M.; Yoon, C.; Kim, H.; Kim, H. The behavior of quartz crystal microbalance in high pressure CO_2. *J. Supercrit. Fluids* **2004**, *29*, 203–212. [CrossRef]
29. Walls, F.L.; Gagnepain, J.-J. Environmental sensitivities of quartz oscillators. *IEEE Trans. Ultrason. Ferroelectr. Freq. Control* **1992**, *39*, 241–249. [CrossRef]
30. Magni, M.; Scaccabarozzi, D.; Saggin, B. Compensation of thermal gradients effects on a quartz crystal microbalance. *Sensors* **2023**, *23*, 24. [CrossRef]

31. Mumyakmaz, B.; Yildiz, B.S.; Akin, T.; Külah, H. A study on the development of a compensation method for humidity effect in QCM sensor responses. *Sens. Actuators B Chem.* **2010**, *147*, 277–282. [CrossRef]
32. Bechmann, R. Frequency-temperature-angle characteristics of AT-type resonators made of natural and synthetic quartz. *Proc. IRE* **1956**, *44*, 1600–1607. [CrossRef]
33. Huang, Q.; Wang, J.; Gan, N.; Ma, T.; Huang, B.; Neubig, B.; Johannsmann, D. An analysis of the thermal behavior and effects of circular quartz crystal resonators for microbalance applications. *IEEE Trans. Ultrason. Ferroelectr. Freq. Control* **2022**, *69*, 2569–2578. [CrossRef]
34. Magni, M.; Saggin, B.; Scaccabarozzi, D.; Tarabini, M.; Palomba, E.; Longobardo, A.; Dirri, F.; Zampetti, E. Temperature sensitivity of a quartz crystal microbalance for TGA in space. In Proceedings of the 2018 5th IEEE International Workshop on Metrology for AeroSpace (MetroAeroSpace), Rome, Italy, 20–22 June 2018; pp. 629–633. [CrossRef]
35. Cooper, M.; Steinem, C.; Janshoff, A. *Piezoelectric Sensors*, 1st ed.; Springer: Berlin, Germany, 2007.
36. Saggin, B.; Tarabini, M.; Scaccabarozzi, D. Infrared Optical Element Mounting Techniques for Wide Temperature Ranges. *Appl. Opt.* **2010**, *49*, 542–548. [CrossRef]
37. European Cooperation for Space Standardization (ECSS). *Thermal Control—Thermal Analysis (ECSS-E-ST-31C)*; ECSS: Noordwijk, The Netherlands, 2008.
38. Breslavsky, D.; Uspenskyi, V.; Mietielov, V.; Senko, A.; Tatarinova, O. Determining the Influence of Thermomechanical Loading on The Measurement Errors of Fiber-Optic Gyroscope. *East.-Eur. J. Enterp. Technol.* **2025**, *2*, 7.
39. García-Pérez, A.; Alonso, G.; Gómez-San-Juan, A.; Pérez-Álvarez, J. Thermoelastic Evaluation of the Payload Module of the ARIEL Mission. *Exp. Astron.* **2022**, *53*, 831–846. [CrossRef]
40. Ivanov, A.Y.; Plokhotnichenko, A.M. A low-temperature quartz microbalance. *Instrum. Exp. Tech.* **2009**, *52*, 308–311. [CrossRef]
41. Scaccabarozzi, D.; Saggin, B.; Magni, M.; Corti, M.G.; Zampetti, E.; Palomba, E.; Longobardo, A.; Dirri, F. Calibration in Cryogenic Conditions of Deposited Thin-Film Thermometers on Quartz Crystal Microbalances. *Sens. Actuators A Phys.* **2021**, *330*, 112878. [CrossRef]
42. Palomba, E.; Colangeli, E.L.; Palumbo, P.; Rotundi, A.; Perrin, J.M.; Bussoletti, E. Performance of Micro-Balances for Dust Flux Measurement. *Adv. Space Res.* **2002**, *29*, 1155–1158. [CrossRef]
43. Klein, M. ECSS-E-30 Mechanical Engineering Standard. *Spacecr. Struct. Mater. Mech. Test.* **2001**, *468*, 479.
44. George, T.; Son, K.A.; Powers, R.A.; Del Castillo, L.Y.; Okojie, R. Harsh Environment Microtechnologies for NASA and Terrestrial Applications. In Proceedings of the IEEE Sensors 2005, Irvine, CA, USA, 30 October–3 November 2005; p. 6. [CrossRef]
45. Goh, G.M. Space Safety Standards in Europe. In *Space Safety Regulations and Standards*; Pelton, J.N., Jakhu, R.S., Eds.; Butterworth-Heinemann: Burlington, VT, USA, 2010; pp. 29–48, ISBN 9781856177528. [CrossRef]
46. Ballato, A.; EerNisse, E.P.; Lukaszek, T. The force-frequency effect in doubly rotated quartz resonators. In Proceedings of the 31st Annual Symposium on Frequency Control, Fort Monmouth, NJ, USA, 1–3 June 1977; pp. 8–16.
47. Chen, F.; Gao, J.; Tian, W. Force-frequency characteristics of multi-electrode quartz crystal resonator cluster. *Sens. Actuators A Phys.* **2018**, *269*, 427–434. [CrossRef]
48. Tian, W.; Sun, Y.; Zhou, H.; Zhao, Q. Force-frequency sensitive character of quartz resonator with same base and different electrode. In *Software Engineering and Knowledge Engineering: Theory and Practice*; Zhang, W., Ed.; Advances in Intelligent and Soft Computing, Volume 162; Springer: Berlin/Heidelberg, Germany, 2012. [CrossRef]
49. Mohammadi, M.M.; Hamedi, M. Force frequency effect in square quartz crystals. *AUT J. Mech. Eng.* **2021**, *5*, 215–226. [CrossRef]
50. Reviakine, I. Quartz Crystal Microbalance in Soft and Biological Interfaces. *Biointerphases* **2024**, *19*, 1. [CrossRef]
51. Mosley, R.J.; Talarico, M.V.; Byrne, M.E. Recent Applications of QCM-D for the Design, Synthesis, and Characterization of Bioactive Materials. *J. Bioact. Compat. Polym.* **2021**, *36*, 261–275. [CrossRef]
52. Scaccabarozzi, D.; Saggin, B.; Magni, M.; Corti, M.G.; Valnegri, P.; Palomba, E.; Longobardo, A.; Dirri, F.; Zampetti, E. Quartz Crystal Microbalances for Space: Design and Testing of a 3D Printed Quasi-Kinematic Support. *Aerospace* **2023**, *10*, 42. [CrossRef]
53. Na Songkhla, S.; Nakamoto, T. Overview of Quartz Crystal Microbalance Behavior Analysis and Measurement. *Chemosensors* **2021**, *9*, 350. [CrossRef]
54. Wang, L. Metal-organic frameworks for QCM-based gas sensors: A review. *Sens. Actuators A Phys.* **2020**, *307*, 111984. [CrossRef]
55. Wang, L.; Song, J.; Yu, C. The utilization and advancement of quartz crystal microbalance (QCM): A mini review. *Microchem. J.* **2024**, *199*, 109967. [CrossRef]
56. Pohanka, M. Quartz crystal microbalance (QCM) sensing materials in biosensors development. *Int. J. Electrochem. Sci.* **2021**, *16*, 211220. [CrossRef]
57. Huang, X.; Chen, Q.; Pan, W.; Yao, Y. Advances in the Mass Sensitivity Distribution of Quartz Crystal Microbalances: A Review. *Sensors* **2022**, *22*, 5112. [CrossRef]
58. Boella, M. Performance of Piezo-Oscillators and the Influence of the Decrement of Quartz on the Frequency Oscillations. *Proc. Inst. Radio. Eng.* **1931**, *19*, 1252–1273. [CrossRef]

59. Arnau, A.; Garcia, J.V.; Jimenez, Y.; Ferrari, V.; Ferrari, M. Improved Electronic Interfaces for Heavy Loaded at Cut Quartz Crystal Microbalance Sensors. In Proceedings of the 2007 IEEE International Frequency Control Symposium Joint with the 21st European Frequency and Time Forum, Geneva, Switzerland, 29 May–1 June 2007; pp. 357–362. [CrossRef]
60. Wersing, W. Small Signal Resonance Methods. In *Piezoelectricity: Evolution and Future of a Technology*; Heywang, W., Lubitz, K., Wersing, W., Eds.; Springer: Berlin/Heidelberg, Germany, 2008; Volume 114, pp. 423–444.